

Creating Quantum Emitters in Hexagonal Boron Nitride Deterministically on Chip-Compatible Substrates

Xiaohui Xu, Zachariah O. Martin, Demid Sychev, Alexei S. Lagutchev, Yong P. Chen, Takashi Taniguchi, Kenji Watanabe, Vladimir M. Shalaev, and Alexandra Boltasseva*



Cite This: *Nano Lett.* 2021, 21, 8182–8189



Read Online

ACCESS |

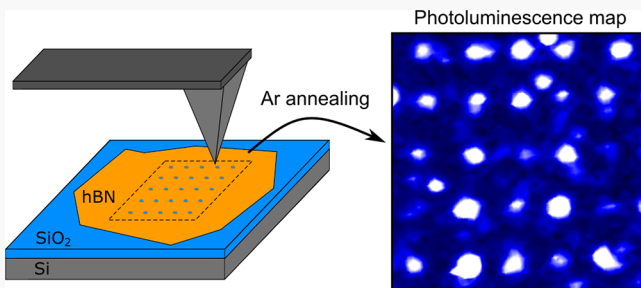
Metrics & More

Article Recommendations

Supporting Information

ABSTRACT: Two-dimensional hexagonal boron nitride (hBN) that hosts room-temperature single-photon emitters (SPEs) is promising for quantum information applications. An important step toward the practical application of hBN is the on-demand, position-controlled generation of SPEs. Strategies reported for deterministic creation of hBN SPEs either rely on substrate nanopatterning that is not compatible with integrated photonics or utilize radiation sources that might introduce unpredictable damage or contamination to hBN. Here, we report a radiation- and lithography-free route to deterministically activate hBN SPEs by nanoindentation with atomic force microscopy (AFM). The method applies to hBN flakes on flat silicon dioxide–silicon substrates that can be readily integrated into on-chip photonic devices. The achieved SPE yields are above 30% for multiple indent sizes, and a maximum yield of 36% is demonstrated for indents around 400 nm. Our results mark an important step toward the deterministic creation and integration of hBN SPEs with photonic and plasmonic devices.

KEYWORDS: hBN, single-photon emitters, atomic force microscopy, nanoindentation, on-chip integration



INTRODUCTION

Solid-state single-photon emitters (SPEs) have received increasing attention in the past decade due to their critical role in quantum information technologies including quantum communication, quantum photonic computing, and quantum sensors.^{1–3} Recently, 2D van der Waals materials such as transition metal dichalcogenides (TMDCs)⁴ and hexagonal boron nitride (hBN)⁵ have been extensively investigated due to their capability to host SPEs. Various types of SPEs operating under ambient conditions have been identified in hBN, with emission ranging from ultraviolet to the near-infrared spectral regime.^{6,7} The atomic-scale thickness of 2D hBN not only enables high-efficiency light extraction but also offers unparalleled advantages for integrating SPEs with plasmonic/photonic structures for hybrid quantum devices.

The practical integration of SPEs in 2D materials requires deterministic creation or activation of emitters at designated locations. Recent studies have reported several methods to fabricate position controlled SPEs in 2D materials based on strain engineering, ion/electron beam irradiation, and so on. Strain-induced SPEs in hBN and TMDCs have been fabricated either by employing a nanostructured substrate (e.g., nanopillars,⁸ nanocones,⁹ etc.)¹⁰ or by deforming 2D materials into a soft polymeric substrate.¹¹ However, both approaches have limited applications in quantum-integrated photonics due to the involvement of patterned substrates or soft polymers. A

similar strategy was utilized in a recent work to obtain hBN SPEs that are not purely strain-induced by growing hBN on dielectric nanopillars using chemical vapor deposition.¹² Aside from the above-mentioned methods, gallium-focused ion beam (FIB) and electron beam have been demonstrated to create position-controlled SPEs in hBN placed on flat substrates.^{13,14} However, the fluorescence contamination induced by high-energy gallium ions could be a potential concern, whereas SPE activation by an electron beam suffers from limited spatial precision (>1 μm).

Herein we propose to deterministically activate room-temperature hBN SPEs by nanoindenting hBN with an AFM probe. The method is demonstrated for hBN flakes on unpatterned SiO₂-coated silicon substrates. AFM probes with diamondlike carbon coatings are used to indent hBN, without notable damage to substrates. The AFM-based method does not introduce fluorescent contaminants, in contrast to radiation- or fabrication-based processes.^{8,12–14} The nanoindentation is followed by argon annealing to fully activate

Received: July 6, 2021

Revised: October 1, 2021

Published: October 4, 2021



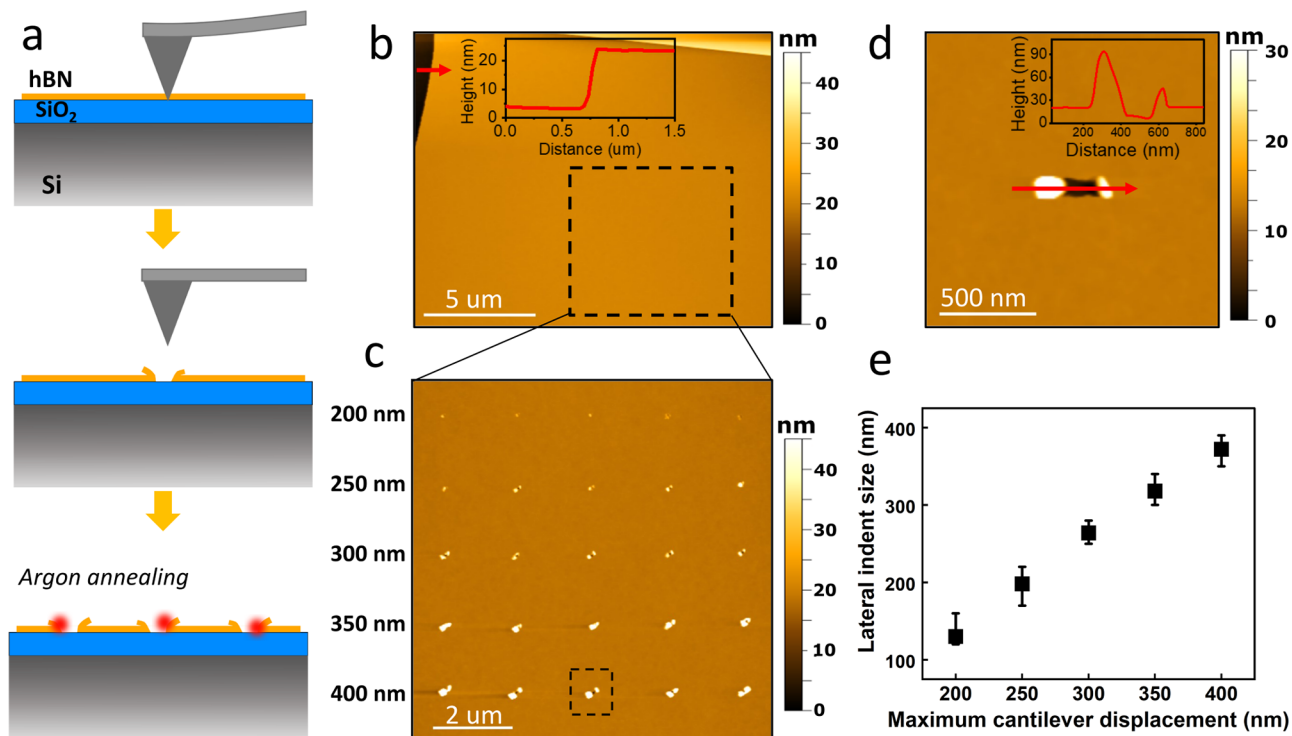


Figure 1. (a) Schematic showing the activation of SPEs in hBN with the AFM nanoindentation technique followed by high-temperature annealing in argon. (b) AFM image showing a thin hBN flake used for demonstrating the nanoindentation process. Upper inset: height profile collected at the flake edge along the red arrow, showing a flake thickness of 19.8 nm. (c) AFM image of the area inside the dashed box in (b) after nanoindentation. The left side lists the values of maximum cantilever displacement (Δz_{\max}) during the indentation for each row of indents. (d) Enlarged view of one specific indent inside the black dashed box in (c), showing a dimple in the flake as well as two broken hBN areas next to the dimple. The image was scanned at 45° with respect to the image in (c) to present the indent along the horizontal direction. Inset: height profile collected across the indent along the red arrow. (e) Dependence of the lateral indent size as a function of the maximum cantilever displacement Δz_{\max} .

SPEs at indented sites. Our results provide a promising route to fabricate site-controlled hBN SPEs on chip-compatible substrates and pave the way to the realization of integrated quantum photonics with hBN. The capability to controllably pattern arrays of quantum emitters also opens exciting possibilities such as realizing a “quantum mirror”^{15–17} and quantum sensors.

RESULTS AND DISCUSSION

A schematic of the proposed nanoindentation technique utilizing AFM is shown in Figure 1a. hBN flakes exfoliated from high-quality hBN crystals are transferred to SiO₂-coated Si substrates. After solvent cleaning, thin flakes with thicknesses around 20 nm and roughnesses below 500 pm are selected for further experiments (see Figure 1b showing an AFM image of a typical hBN flake used for demonstrating the nanoindentation effect). In the AFM contact mode, the cantilever is brought into contact with hBN and then gets indented into the flake with further cantilever displacement along the vertical direction. By adjusting the maximum cantilever displacement (Δz_{\max}), indents with varying lateral sizes are obtained (Figure 1c). Scanning over a specific indent reveals that the indented structure is composed of a dip in hBN as well as two bent hBN pieces resulting from the AFM probe impact (Figure 1d). To demonstrate how the indent size scales with the cantilever displacement, we measured the lateral sizes of all indents presented in Figure 1c as a function of Δz_{\max} . The method used to determine lateral indent sizes could be found in the Supporting Information. As illustrated in Figure

1e, the lateral indent size scales almost linearly with Δz_{\max} in the tested Δz_{\max} range. We note that changing Δz_{\max} mainly affects the lateral dimension rather than the depth of resulting indents. The indentation typically creates dimples with depths less than or comparable to the hBN flake thickness even for the largest indents tested (Figure S2). This implies that our developed indentation procedure “pokes” hBN without deforming or damaging the substrate.

Our findings are in contrast with reported indentation experiments on TMDCs,^{11,18} where TMDC layers are completely deformed into indented dips with depths depending on Δz_{\max} without being torn apart by cantilevers. One reason can be attributed to our relatively rigid substrate (SiO₂-on-Si) that is not amenable to deformation, while in ref 11, a soft polymer substrate is used to facilitate the downward deformation of TMDC. The difference between hBN and TMDCs in their mechanical properties could also play an important role. High-quality hBN thin films around 15 nm thick have a reported Young’s modulus of 1.2 TPa,¹⁹ more than 4 times larger than that of TMDCs.²⁰ This indicates that hBN is stiffer than TMDCs thus tends to break more easily before significant deformation. An additional factor is the different types of cantilevers used among studies in terms of coating material, tip radius, and so on, which might lead to varied sample responses. Here, the indentation of hBN without notable damage into substrates is, in fact, a unique advantage in practical applications where hBN flakes are placed on photonic components such as waveguides, cavities, and so on.

After the nanoindentation, hBN samples are annealed in argon at 1000 °C for 30 min to achieve efficient SPE

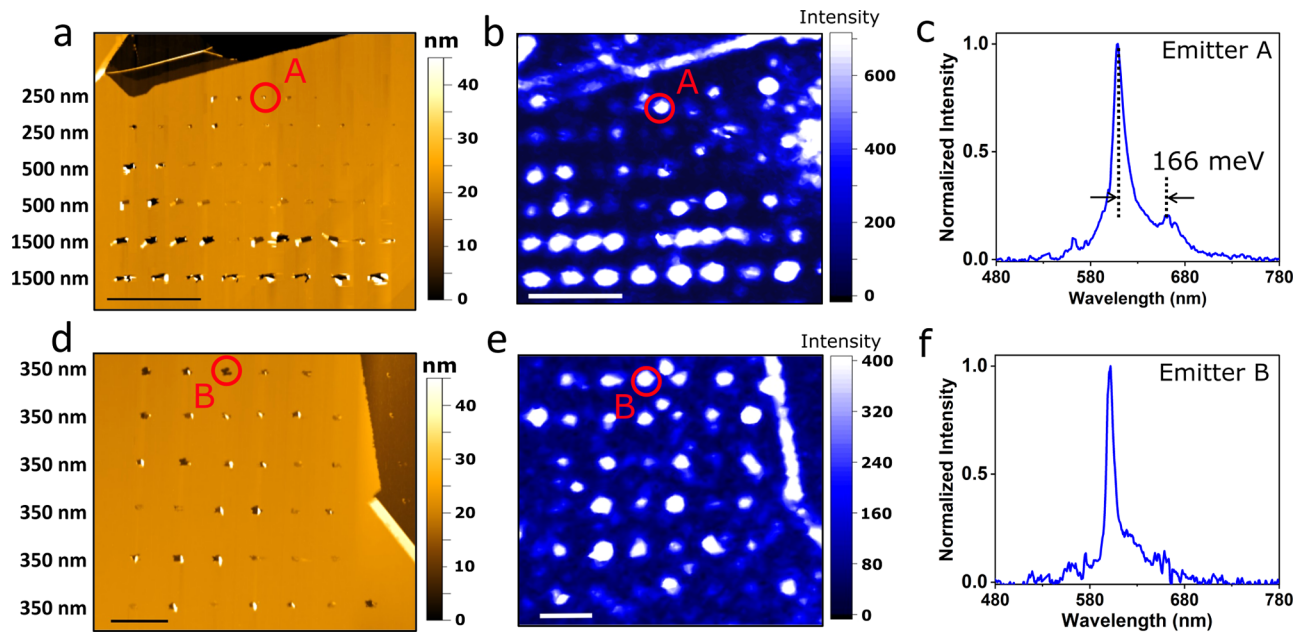


Figure 2. (a) AFM image of the first flake after nanoindentation. Three groups of indents (with two rows in each group) are created with Δz_{\max} of 250, 500, and 1500 nm, as indicated on the left of each row. From top to bottom, the number of indents in each row is 5, 11, 11, 9, 10, and 8, respectively. Scale bar: 5 μm . (b) Photoluminescence (PL) map from the same area shown in (a) after Ar annealing, obtained at a laser power of 800 μW . Scale bar: 5 μm . (c) Background-subtracted spectrum from representative emitter A circled in (a) and (b). A phonon sideband (PSB) that is 166 meV away from the zero-phonon line (ZPL) at 608 nm is identified. (d) AFM image of the second flake after nanoindentation. Six rows of indents are created with the same Δz_{\max} of 350 nm. From top to bottom, the number of indents in each row is 5, 6, 6, 6, 6, and 7, respectively. Scale bar: 2 μm . (e) PL map of the same area shown in (d) after Ar annealing. Scale bar: 2 μm . (f) Background-subtracted spectrum from representative emitter B circled in (d) and (e), showing a sharp ZPL line centered at 602 nm.

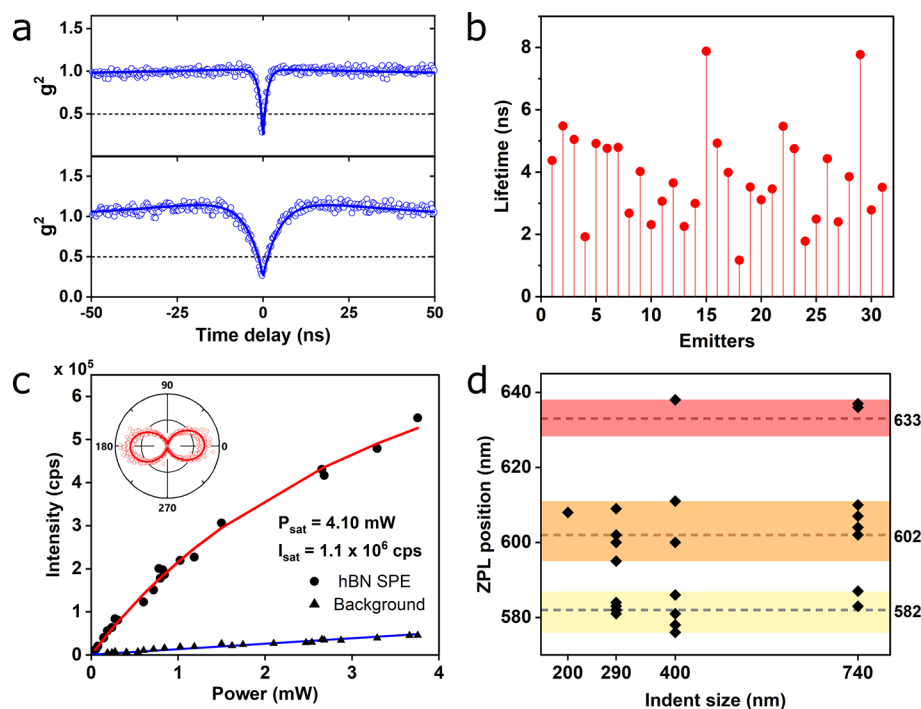


Figure 3. Photophysical properties of hBN emitters. (a) Second-order autocorrelation measurements of emitters A and B. Blue circles are experimental data, while blue solid lines are fitted curves using the three-level model. Both emitters show $g^2(0) < 0.5$ indicative of single-photon emission. (b) Distribution of radiative lifetimes from all 31 hBN SPEs, extracted from $g^2(t)$ fitting. The numbering of SPEs can be found in Figure S6. (c) Fluorescence saturation curve of a typical SPE with a saturation count of 1.1 Mcps. Inset: Emission polarization plot of an hBN SPE. (d) Distribution of ZPLs for 26 photostable SPEs, revealing three classes of emitters with ZPLs at 582 ± 6 nm, 602 ± 9 nm, and 633 ± 5 nm, respectively. The shaded bands are guides to the eye.

activation.⁷ In the following experiments, two types of AFM-indent hBN samples are annealed and characterized: one with varied indentation sizes on the same flake to investigate the correlation between indent sizes and SPE generation and another with one indent size combining a high SPE yield and indentation precision. Figure 2a shows an hBN flake that has been indented with three different Δz_{\max} . Here, relatively large step sizes in Δz_{\max} are used compared to the demonstration in Figure 1, which helps us to extract the dependence of SPEs on the lateral indent size in a broader size range. The lateral size distribution of all indents can be found in Figure S3, and average indent sizes of 200, 400, and 750 nm are measured in the three groups. For indents as large as 750 nm, the corresponding indentation depths are still comparable to the hBN flake thickness (Figure S3d), again confirming that our technique has negligible impact on substrates. Overall, our indentation procedure can produce a designated indent size with decent repeatability. To further reduce the error in indent size at a given Δz_{\max} , one can explore the rich parameters in the nanoindentation procedure, such as the indentation trigger point, cantilever extension/retraction velocity, and so on.

After Ar annealing, the flake is scanned with our lab-built confocal microscope at room temperature. A continuous-wave laser (532 nm) is used for scanning and the photoluminescence (PL) map from the AFM-indented area is collected (Figure 2b). Bright isolated spots are identified at positions corresponding to the indented areas, with low background emission rates being recorded away from these spots. Spectroscopic measurements reveal that PL spectra from those bright spots typically show well-defined emission peaks on top of a low background. The spectrum of representative emitter A is presented in Figure 2c: A sharp emission peak at 608 nm (2.04 eV) matches one of the reported zero-phonon lines (ZPLs) of hBN emitters (602 nm).⁷ A broader peak that is \sim 166 meV away from the ZPL is recognized as a phonon sideband (PSB) corresponding to the in-plane optical phonons of hBN.^{7,21–23} This confirms that our technique is capable of activating room-temperature emitters in hBN at indents as small as 200 nm in size.

Another important observation is that the yield of bright emission spots increases monotonically with indent size (Figure 2b). While a high emitter yield would be desired, it is also preferable to work with emitters from smaller indents such that the on-chip integration of emitters could be achieved with better precision.^{24–26} To balance the above two factors, we nanoindented another flake with Δz_{\max} of 350 nm. Advantages of this specific Δz_{\max} will be discussed later. The developed nanoindentation procedure has reproduced arrays of indents with comparable sizes (Figures 2d and S4), with an average lateral size of 290 nm. The PL map of this area (Figure 2e) shows arrays of bright emission spots that match well with the AFM indentation pattern. The emission spectrum of typical emitter B in the area (Figure 2f) again exhibits a sharp ZPL emission centered at 602 nm (2.06 eV).

After confirming the existence of hBN emitters at nanoindented sites on both flakes above, we next evaluated their single-photon purity using a Hanbury, Brown, and Twiss (HBT) setup that measures the second-order autocorrelation functions $g^2(t)$ of emitters A and B (Figure 3a). Both emitters have $g^2(0) < 0.5$ at zero delay time, confirming that they are single-photon sources. Their limited single-photon purity ($g^2(0) > 0.1$) is most likely due to the background emission from organic residue contaminants (Figure S5). Treatments

such as air annealing and UV ozone cleaning could be explored as postprocessing routes to improve the purity of such emitters.²⁷ The experimental $g^2(t)$ data can be fit well with a three-level model:^{5,28}

$$g^2(t) = 1 - (1 + a) e^{-|t|/\tau_1} + a e^{-|t|/\tau_2}$$

where a is the photon bunching amplitude and τ_1 and τ_2 are lifetimes of the excited and metastable states, respectively. After careful examination, 31 SPEs were identified out of all the indented sites from the two hBN flakes above (Figure S6). The radiative decay lifetimes of all SPEs extracted from $g^2(t)$ range from 1.17 to 7.88 ns with an average lifetime of 3.86 ns (Figure 3b). Our observation agrees with the typical lifetimes reported for room-temperature hBN SPEs.^{7,29} To measure emitter brightness, the PL intensities at a series of incident laser powers are recorded and then fit using a first-order saturation model: $I = I_{\text{sat}} P / (P + P_{\text{sat}})$, where $P(P_{\text{sat}})$ and $I(I_{\text{sat}})$ are the incident (saturated) power and PL intensity, respectively. Figure 3c shows the fitted saturation curve of one bright emitter that saturates at 4.1 mW with a saturation intensity of 1.1 Mcps, comparable to the brightest hBN emitters created by other techniques.^{7,13,14,30} SPEs in this work typically exhibit linearly polarized emission (Figure 3c, inset), indicating an atomic defect with the in-plane dipole moment.²⁹ However, no notable correlation is found between the orientation of the emission dipole and the elongation of the lateral indent. (Figure S7). The photostability of SPEs is also examined by recording their PL time traces. It is observed that \sim 50% of the SPEs maintain stable emission during the optical characterization, while 40% and 10% exhibit blinking and photobleaching behaviors (Figure S8). Blinking has been commonly observed in hBN SPEs^{12,21,31} as well as in other types of solid-state SPEs.^{32–34} Specifically, hBN SPEs created by deterministic techniques have been reported to show blinking,^{8,12,13} despite high-temperature annealing treatments which are proved to improve emission stability.³⁰ This is likely related to the complex local environment near SPEs after the hBN lattice gets modified by strain, electron/ion irradiation, and so on. Strategies to effectively improve the photostability of deterministically formed hBN SPEs are therefore highly desirable.

Figure 3d summarizes the distribution of ZPLs for all photostable SPEs from AFM-indented sites. The emitters can be classified into three groups, with ZPLs centered at 582 ± 6 nm, 602 ± 9 nm and 633 ± 5 nm, all of which match the previously reported ZPLs of hBN SPEs in the visible spectral range.⁷ Unlike SPEs created by other top-down techniques where a dominating portion of emitters show ZPLs at wavelengths shorter than 590 nm,^{8,13} nearly 50% of emitters created with our technique exhibit ZPLs around 602 nm, and another 40% show emission centered around 582 nm. Some SPEs (35%) show PSBs in their spectra that are 167 ± 10 meV away from the corresponding ZPLs (Figure S9), in agreement with previous reports.^{35–38} The relatively narrow distribution of ZPLs implies that our technique is promising for deterministically creating hBN SPEs with predictable emission wavelengths.

To determine if there exist a correlation between the lifetime or ZPL wavelength of identified SPEs and the corresponding indent sizes, we plotted the distribution of the lifetime and the ZPL wavelength of hBN SPEs as a function of the lateral indent size (Supporting Information). As shown in Figure S10, no notable correlations are observed, which indicates that SPEs

created at indents with varied sizes have consistent optical properties.

Aside from SPEs, we also found emitters that possess some degrees of antibunching ($0.5 < g^2(0) < 1$). Considering the low fluorescence background of our samples, such emitters are most likely composed of more than one SPE within spatially unresolvable spots.³⁹ Spectra collected from these emitters typically show broader emission peaks or multipeaked emission, confirming the existence of multiple SPEs that cannot be individually addressed (Figure S11). To demonstrate the correlation between $g^2(0)$ and indent size of corresponding emitters, we summarized the distribution of $g^2(0)$ for emitters showing antibunched emission ($g^2(0) < 1$) as a function of corresponding indent sizes. Emitters from both hBN flakes above, with average indent sizes of 200, 290, 400, and 740 nm, are included for statistical purposes. SPEs ($g^2(0) < 0.5$) are found from all four groups of indents, whereas clustered emitters ($0.5 < g^2(0) < 1$) are only found from indents with sizes of ≥ 290 nm (Figure 4). After dividing the

effective generation of clustered emitters in larger indents could be useful as well, for example, for sensing applications.

We now discuss the formation mechanisms of hBN emitters created by AFM nanoindentation and their potential applications. First, we note that no stable emitters are observed on AFM-indented hBN flakes before argon annealing. The necessity of high-temperature annealing for SPE activation indicates that the emitters are most likely vacancy-related defects as vacancy diffusion typically dominates at high temperatures.⁴⁰ To validate this, we performed a control experiment by annealing additional nanoindented hBN samples in argon at a lower temperature, namely, 800 °C (see the Supporting Information for details). As seen in Figure S12, SPEs formed with a much lower yield compared to that of hBN flakes annealed at 1000 °C. This confirms that the formation of SPEs is less favorable at lower annealing temperatures likely due to the reduced vacancy diffusion rate. Our observation agrees with ref 7 where a monotonic increase in emitter yield is reported as annealing temperature increases. Nevertheless, further increasing the annealing temperature above 1000 °C is not preferred in practice considering the degradation of involved materials. Other post-AFM treatments such as plasma etching^{30,41,42} could be explored as alternative ways to achieve higher SPE yields in the future.

The diffraction-limited resolution of the confocal microscope has prevented us from locating observed hBN SPEs with nanoscale precision. Nevertheless, we infer that SPEs are most likely formed either at the edge of indented dips or on the bent, delaminated hBN areas next to the dips. The former favors SPE formation as defects tend to accumulate at structure/grain boundaries,^{13,43} while the latter could activate strain-induced SPEs due to the large curvature near the bent hBN areas. It is highly possible that both mechanisms play a role here, resulting in higher SPE yields than those reported for the at-the-boundary creation or strain engineering.^{8,13} To better locate such SPEs, one can use a near-field scanning optical microscope,⁴⁴ scanning antenna microscope,⁴⁵ or combined optical microscope–AFM setup⁴⁶ to get correlated PL and topographical maps. The obtained knowledge would also help to achieve a better control over the number of emitters formed at one indent site by optimizing the morphology of indent structures.

One of the most important advantages of AFM-indented hBN SPEs is the combined high SPE yield and high-precision position control. As demonstrated here, a SPE yield of 32% is obtained for indents smaller than 300 nm, which sets the new record for deterministic creation of hBN SPEs on non-structured substrates. It also needs to be emphasized that indents created by AFM feature sharp, well-defined edges, in contrast to holes/spots induced by radiation methods that typically have poorly defined boundaries due to the diffuse nature of radiation beams. Furthermore, our technique can be extended to hBN flakes with various thicknesses by simply adjusting the indentation parameters, making it more versatile than strain engineering with structured substrates as the latter typically requires thin hBN films to achieve desired deformation.

The position-controlled creation of hBN SPEs with AFM nanoindentation could be promising for various quantum photonic applications. For example, it enables the efficient integration of hBN SPEs with photonic waveguides or cavities by creating SPEs at desired positions, in contrast to previous

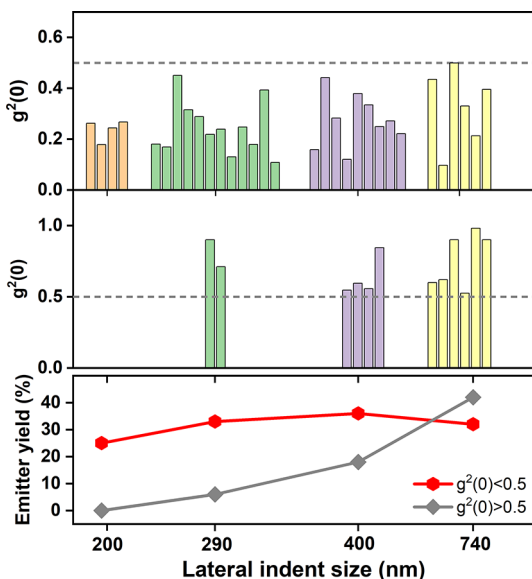


Figure 4. Top and middle: $g^2(0)$ values of SPEs ($g^2(0) < 0.5$, top) and clustered SPEs ($0.5 < g^2(0) < 1$, middle) as a function of corresponding indent sizes. Bottom: Yield of SPE and clustered emitters as a function of lateral indent size, calculated by dividing the number of emitters over the total number of indents created for each indent size.

number of emitters with the total number of indents in each group, we obtained the emitter yields of clustered emitters and SPEs for different indent sizes (bottom panel in Figure 4). The yield of clustered emitters shows a monotonic increase with indent sizes, from 0% for 200 nm sized indents to over 40% for an indent size of 740 nm. In contrast, the SPE yield first increases with indent sizes, from 25% for indents of 200 nm up to 36% for indents of 400 nm, and it then drops for indents larger than 400 nm. The SPE yields for indents of 290 nm (32%) and 400 nm (36%) are, to the best of our knowledge, among the highest values ever reported for hBN SPEs created by top-down methods including FIB and nanopillar arrays.^{8,13} Specifically, indents around 290 nm combine a high SPE yield and a relatively small feature size, making them promising for the deterministic quantum integration of hBN SPEs. The

studies where hBN SPEs are coupled to photonic structures either randomly^{25,47–49} or more deterministically, yet with extensive alignment efforts.⁵⁰ The developed technique also offers a great potential for coupling hBN SPEs to plasmonic nanostructures for strong emission enhancement.⁵¹ Compared to randomly activated SPEs in hBN that do not possess recognizable topographical features, SPEs near the nanosized indents make it possible to deterministically assemble plasmonic cavity/antenna structures^{52,53} with high SPE coupling efficiency. In addition, AFM-induced hBN SPEs could be used in other studies that might benefit from deterministic emitter coupling, such as sensing, emission tuning,^{54,55} quantum nonlinear optics,^{56,57} and more.

CONCLUSION

We demonstrated a new route to deterministically create room-temperature SPEs in hBN utilizing AFM nanoindentation. The technique is applied to hBN flakes on unpatterned SiO₂-on-Si substrates. By tuning the indentation parameters, indents with various lateral sizes are obtained without notable damage of the substrate. HBN SPEs are activated near the indents after a post-AFM annealing step. Over 80% of the SPEs show ZPLs around 583 and 602 nm. A maximum SPE yield of 36% is obtained for an indent size of 400 nm, and indents around 290 nm give a comparably high SPE yield. Our method involves no lithographic or other patterning steps; hence, fabrication-induced fluorescence contamination is avoided. While the nature of these indentation-induced SPEs has to be studied in more detail, it is inferred that the creation of structural edges and highly strained hBN areas near the indents could be responsible for the high SPE yield. The efficient SPE activation on flat, chip-compatible substrates with high precision allows controlled coupling of hBN SPEs with plasmonic/photonic devices for various quantum applications. Therefore, our results open exciting avenues toward the on-chip deterministic integration of hBN SPEs and future on-chip quantum photonic devices.

ASSOCIATED CONTENT

Supporting Information

The Supporting Information is available free of charge at <https://pubs.acs.org/doi/10.1021/acs.nanolett.1c02640>.

Details of sample preparation and experimental setup. Measurement and determination of indent size, dependence of indentation depth on the maximum cantilever displacement, additional data of hBN flakes used for optical measurements, and control experiment with hBN flakes annealed at 800 °C (PDF)

AUTHOR INFORMATION

Corresponding Author

Alexandra Boltasseva – School of Materials Engineering, Purdue University, West Lafayette, Indiana 47906, United States; School of Electrical and Computer Engineering, Purdue University, West Lafayette, Indiana 47906, United States; orcid.org/0000-0001-8905-2605; Email: aeb@purdue.edu

Authors

Xiaohui Xu – School of Materials Engineering, Purdue University, West Lafayette, Indiana 47906, United States; orcid.org/0000-0003-0369-3917

Zachariah O. Martin – School of Electrical and Computer Engineering, Purdue University, West Lafayette, Indiana 47906, United States

Demid Sychev – School of Electrical and Computer Engineering, Purdue University, West Lafayette, Indiana 47906, United States

Alexei S. Lagutchev – School of Electrical and Computer Engineering, Purdue University, West Lafayette, Indiana 47906, United States

Yong P. Chen – School of Electrical and Computer Engineering and Department of Physics and Astronomy, Purdue University, West Lafayette, Indiana 47906, United States; Department of Physics and Astronomy, Aarhus University, Aarhus 8000, Denmark

Takashi Taniguchi – National Institute for Materials Science, Tsukuba, Ibaraki 305-0047, Japan; orcid.org/0000-0002-1467-3105

Kenji Watanabe – National Institute for Materials Science, Tsukuba, Ibaraki 305-0047, Japan; orcid.org/0000-0003-3701-8119

Vladimir M. Shalaev – School of Electrical and Computer Engineering, Purdue University, West Lafayette, Indiana 47906, United States

Complete contact information is available at:

<https://pubs.acs.org/10.1021/acs.nanolett.1c02640>

Author Contributions

X.X. conceived the idea and designed the experiment. D.S. transferred hBN flakes to designated substrates. X.X. performed the AFM nanoindentation experiments. Z.O.M. performed the argon annealing experiments. Z.O.M., X.X., and D.S. conducted the optical characterization experiments. X.X. wrote the initial draft of the paper. V.M.S. and A.B. supervised the project. All authors contributed in the discussion and writing of the paper.

Notes

The authors declare no competing financial interest.

ACKNOWLEDGMENTS

The authors acknowledge S. I. Bogdanov, A. Senichev, and A. B. Solanki for helpful discussions on the optical characterization of hBN SPEs. This work is supported by the U.S. Department of Energy (DOE), Office of Science through the Quantum Science Center (QSC), a National Quantum Information Science Research Center, and National Science Foundation Award 2015025-ECCS.

REFERENCES

- (1) O'Brien, J. L.; Furusawa, A.; Vučković, J. Photonic Quantum Technologies. *Nat. Photonics* **2009**, *3*, 687–695.
- (2) Aharonovich, I.; Englund, D.; Toth, M. Solid-State Single-Photon Emitters. *Nat. Photonics* **2016**, *10*, 631–641.
- (3) Atatüre, M.; Englund, D.; Vamivakas, N.; Lee, S. Y.; Wrachtrup, J. Material Platforms for Spin-Based Photonic Quantum Technologies. *Nature Reviews Materials* **2018**, *3*, 38–51.
- (4) He, Y. M.; Clark, G.; Schaibley, J. R.; He, Y.; Chen, M. C.; Wei, Y. J.; Ding, X.; Zhang, Q.; Yao, W.; Xu, X.; Lu, C. Y.; Pan, J. W. Single Quantum Emitters in Monolayer Semiconductors. *Nat. Nanotechnol.* **2015**, *10*, 497–502.
- (5) Tran, T. T.; Bray, K.; Ford, M. J.; Toth, M.; Aharonovich, I. Quantum Emission from Hexagonal Boron Nitride Monolayers. *Nat. Nanotechnol.* **2016**, *11*, 37–41.

(6) Bourrelier, R.; Meuret, S.; Tararan, A.; Stéphan, O.; Kociak, M.; Tizei, L. H. G.; Zobelli, A. Bright UV Single Photon Emission at Point Defects in H-BN. *Nano Lett.* **2016**, *16*, 4317–4321.

(7) Tran, T. T.; Elbadawi, C.; Totonjian, D.; Lobo, C. J.; Gross, G.; Moon, H.; Englund, D. R.; Ford, M. J.; Aharonovich, I.; Toth, M. Robust Multicolor Single Photon Emission from Point Defects in Hexagonal Boron Nitride. *ACS Nano* **2016**, *10*, 7331–7338.

(8) Proscia, N. V.; Shotan, Z.; Jayakumar, H.; Reddy, P.; Cohen, C.; Dollar, M.; Alkauskas, A.; Doherty, M.; Meriles, C. A.; Menon, V. M. Near-Deterministic Activation of Room Temperature Quantum Emitters in Hexagonal Boron Nitride. *Optica* **2018**, *5*, 1128–1134.

(9) Li, H.; Contryman, A. W.; Qian, X.; Ardakani, S. M.; Gong, Y.; Wang, X.; Weisse, J. M.; Lee, C. H.; Zhao, J.; Ajayan, P. M.; Li, J.; Manoharan, H. C.; Zheng, X. Optoelectronic Crystal of Artificial Atoms in Strain-Textured Molybdenum Disulphide. *Nat. Commun.* **2015**, *6*, 7381.

(10) Tonndorf, P.; Schmidt, R.; Schneider, R.; Kern, J.; Buscema, M.; Steele, G. A.; Castellanos-Gomez, A.; van der Zant, H. S. J.; Michaelis de Vasconcellos, S.; Bratschitsch, R. Single-Photon Emission from Localized Excitons in an Atomically Thin Semiconductor. *Optica* **2015**, *2*, 347–352.

(11) Rosenberger, M. R.; Dass, C. K.; Chuang, H. J.; Sivaram, S. V.; McCreary, K. M.; Hendrickson, J. R.; Jonker, B. T. Quantum Calligraphy: Writing Single-Photon Emitters in a Two-Dimensional Materials Platform. *ACS Nano* **2019**, *13*, 904–912.

(12) Li, C.; Mendelson, N.; Ritika, R.; Chen, Y.-L.; Xu, Z.-Q.; Toth, M.; Aharonovich, I. Scalable and Deterministic Fabrication of Quantum Emitter Arrays from Hexagonal Boron Nitride. *Nano Lett.* **2021**, *21*, 3626–3632.

(13) Ziegler, J.; Klaiss, R.; Blaikie, A.; Miller, D.; Horowitz, V. R.; Aleman, B. J. Deterministic Quantum Emitter Formation in Hexagonal Boron Nitride via Controlled Edge Creation. *Nano Lett.* **2019**, *19*, 2121–2127.

(14) Fournier, C.; Plaud, A.; Roux, S.; Pierret, A.; Rosticher, M.; Watanabe, K.; Taniguchi, T.; Buil, S.; Quelin, X.; Barjon, J.; et al. Position-Controlled Quantum Emitters with Reproducible Emission Wavelength in Hexagonal Boron Nitride. *Nat. Commun.* **2021**, *12*, 3779.

(15) Shahmoon, E.; Wild, D. S.; Lukin, M. D.; Yelin, S. F. Cooperative Resonances in Light Scattering from Two-Dimensional Atomic Arrays. *Phys. Rev. Lett.* **2017**, *118*, 113601.

(16) Rui, J.; Wei, D.; Rubio-Abadal, A.; Hollerith, S.; Zeiher, J.; Stamper-Kurn, D. M.; Gross, C.; Bloch, I. A Subradiant Optical Mirror Formed by a Single Structured Atomic Layer. *Nature* **2020**, *583*, 369–374.

(17) Bettles, R. J.; Gardiner, S. A.; Adams, C. S. Enhanced Optical Cross Section via Collective Coupling of Atomic Dipoles in a 2D Array. *Phys. Rev. Lett.* **2016**, *116*, 103602.

(18) Kumar, P.; Balakrishnan, V. Nanosculpting of Atomically Thin 2D Materials for Site-Specific Photoluminescence Modulation. *Adv. Opt. Mater.* **2018**, *6*, 1701284.

(19) Kim, S. M.; Hsu, A.; Park, M. H.; Chae, S. H.; Yun, S. J.; Lee, J. S.; Cho, D. H.; Fang, W.; Lee, C.; Palacios, T.; Dresselhaus, M.; Kim, K. K.; Lee, Y. H.; Kong, J. Synthesis of Large-Area Multilayer Hexagonal Boron Nitride for High Material Performance. *Nat. Commun.* **2015**, *6*, 8662.

(20) Falin, A.; Holwill, M.; Lv, H.; Gan, W.; Cheng, J.; Zhang, R.; Qian, D.; Barnett, M. R.; Santos, E. J. G.; Novoselov, K. S.; Tao, T.; Wu, X.; Li, L. H. Mechanical Properties of Atomically Thin Tungsten Dichalcogenides: WS₂, WSe₂, and WTe₂. *ACS Nano* **2021**, *15*, 2600–2610.

(21) Shotan, Z.; Jayakumar, H.; Considine, C. R.; Mackoit, M.; Fedder, H.; Wrachtrup, J.; Alkauskas, A.; Doherty, M. W.; Menon, V. M.; Meriles, C. A. Photoinduced Modification of Single-Photon Emitters in Hexagonal Boron Nitride. *ACS Photonics* **2016**, *3*, 2490–2496.

(22) Jung, S.; Park, M.; Park, J.; Jeong, T. Y.; Kim, H. J.; Watanabe, K.; Taniguchi, T.; Ha, D. H.; Hwang, C.; Kim, Y. S. Vibrational Properties of H-BN and h-BN-Graphene Heterostructures Probed by Inelastic Electron Tunneling Spectroscopy. *Sci. Rep.* **2015**, *5*, 16642.

(23) Wang, Q.; Zhang, Q.; Zhao, X.; Luo, X.; Wong, C. P. Y.; Wang, J.; Wan, D.; Venkatesan, T.; Pennycook, S. J.; Loh, K. P.; Eda, G.; Wee, A. T. S. Photoluminescence Upconversion by Defects in Hexagonal Boron Nitride. *Nano Lett.* **2018**, *18*, 6898–6905.

(24) Caldwell, J. D.; Aharonovich, I.; Cassabois, G.; Edgar, J. H.; Gil, B.; Basov, D. N. Photonics with Hexagonal Boron Nitride. *Nature Reviews Materials* **2019**, *4*, 552–567.

(25) Kim, S.; Duong, N. M. H.; Nguyen, M.; Lu, T. J.; Kianinia, M.; Mendelson, N.; Solntsev, A.; Bradac, C.; Englund, D. R.; Aharonovich, I. Integrated on Chip Platform with Quantum Emitters in Layered Materials. *Adv. Opt. Mater.* **2019**, *7*, 1901132.

(26) Proscia, N. V.; Jayakumar, H.; Ge, X.; Lopez-Morales, G.; Shotan, Z.; Zhou, W.; Meriles, C. A.; Menon, V. M. Microcavity-Coupled Emitters in Hexagonal Boron Nitride. *Nanophotonics* **2020**, *9*, 2937–2944.

(27) Li, C.; Xu, Z. Q.; Mendelson, N.; Kianinia, M.; Toth, M.; Aharonovich, I. Purification of Single-Photon Emission from HBN Using Post-Processing Treatments. *Nanophotonics* **2019**, *8*, 2049–2055.

(28) Martínez, L. J.; Pelini, T.; Waselowski, V.; Maze, J. R.; Gil, B.; Cassabois, G.; Jacques, V. Efficient Single Photon Emission from a High-Purity Hexagonal Boron Nitride Crystal. *Phys. Rev. B: Condens. Matter Mater. Phys.* **2016**, *94*, No. 121405(R).

(29) Exarhos, A. L.; Hopper, D. A.; Grote, R. R.; Alkauskas, A.; Bassett, L. C. Optical Signatures of Quantum Emitters in Suspended Hexagonal Boron Nitride. *ACS Nano* **2017**, *11*, 3328–3336.

(30) Xu, Z. Q.; Elbadawi, C.; Tran, T. T.; Kianinia, M.; Li, X.; Liu, D.; Hoffman, T. B.; Nguyen, M.; Kim, S.; Edgar, J. H.; Wu, X.; Song, L.; Ali, S.; Ford, M.; Toth, M.; Aharonovich, I. Single Photon Emission from Plasma Treated 2D Hexagonal Boron Nitride. *Nanoscale* **2018**, *10*, 7957–7965.

(31) Li, X.; Shepard, G. D.; Cupo, A.; Camporeale, N.; Shayan, K.; Luo, Y.; Meunier, V.; Strauf, S. Nonmagnetic Quantum Emitters in Boron Nitride with Ultranarrow and Sideband-Free Emission Spectra. *ACS Nano* **2017**, *11*, 6652–6660.

(32) Tang, J.; Marcus, R. A. Mechanisms of Fluorescence Blinking in Semiconductor Nanocrystal Quantum Dots. *J. Chem. Phys.* **2005**, *123*, 054704.

(33) Ai, N.; Walden-Newman, W.; Song, Q.; Kallikatos, S.; Strauf, S. Suppression of Blinking and Enhanced Exciton Emission from Individual Carbon Nanotubes. *ACS Nano* **2011**, *5*, 2664–2670.

(34) Bradac, C.; Gaebel, T.; Naidoo, N.; Sellars, M. J.; Twamley, J.; Brown, L. J.; Barnard, A. S.; Plakhotnik, T.; Zvyagin, A. V.; Rabreau, J. R. Observation and Control of Blinking Nitrogen-Vacancy Centres in Discrete Nanodiamonds. *Nat. Nanotechnol.* **2010**, *5*, 345–349.

(35) Boll, M. K.; Radko, I. P.; Huck, A.; Andersen, U. L. Photophysics of Quantum Emitters in Hexagonal Boron-Nitride Nano-Flakes. *Opt. Express* **2020**, *28*, 7475.

(36) Feldman, M. A.; Puretzky, A.; Lindsay, L.; Tucker, E.; Briggs, D. P.; Evans, P. G.; Haglund, R. F.; Lawrie, B. J. Phonon-Induced Multicolor Correlations in HBN Single-Photon Emitters. *Phys. Rev. B: Condens. Matter Mater. Phys.* **2019**, *99*, No. 020101(R).

(37) Kianinia, M.; Regan, B.; Tawfik, S. A.; Tran, T. T.; Ford, M. J.; Aharonovich, I.; Toth, M. Robust Solid-State Quantum System Operating at 800 K. *ACS Photonics* **2017**, *4*, 768–773.

(38) Jungwirth, N. R.; Calderon, B.; Ji, Y.; Spencer, M. G.; Flatté, M. E.; Fuchs, G. D. Temperature Dependence of Wavelength Selectable Zero-Phonon Emission from Single Defects in Hexagonal Boron Nitride. *Nano Lett.* **2016**, *16*, 6052–6057.

(39) Brouri, R.; Beveratos, A.; Poizat, J.-P.; Grangier, P. Photon Antibunching in the Fluorescence of Individual Color Centers in Diamond. *Opt. Lett.* **2000**, *25*, 1294.

(40) Pezzagna, S.; Rogalla, D.; Wildanger, D.; Meijer, J.; Zaitsev, A. Creation and Nature of Optical Centres in Diamond for Single-Photon Emission—Overview and Critical Remarks. *New J. Phys.* **2011**, *13*, 035024.

(41) Sevak Singh, R.; Yingjie Tay, R.; Leong Chow, W.; Hon Tsang, S.; Mallick, G.; Tong Teo, E. H. Band Gap Effects of Hexagonal Boron Nitride Using Oxygen Plasma. *Appl. Phys. Lett.* **2014**, *104*, 163101.

(42) Petracic, M.; Peter, R.; Kavre, I.; Li, L. H.; Chen, Y.; Fan, L. J.; Yang, Y. W. Decoration of Nitrogen Vacancies by Oxygen Atoms in Boron Nitride Nanotubes. *Phys. Chem. Chem. Phys.* **2010**, *12*, 15349–15353.

(43) Choi, S.; Tran, T. T.; Elbadawi, C.; Lobo, C.; Wang, X.; Juodkazis, S.; Seniutinas, G.; Toth, M.; Aharonovich, I. Engineering and Localization of Quantum Emitters in Large Hexagonal Boron Nitride Layers. *ACS Appl. Mater. Interfaces* **2016**, *8*, 29642–29648.

(44) Dürig, U.; Pohl, D. W.; Rohner, F. Near-Field Optical-Scanning Microscopy. *J. Appl. Phys.* **1986**, *59*, 3318–3327.

(45) Palombo Blascetta, N.; Liebel, M.; Lu, X.; Taniguchi, T.; Watanabe, K.; Efetov, D. K.; Van Hulst, N. F. Nanoscale Imaging and Control of Hexagonal Boron Nitride Single Photon Emitters by a Resonant Nanoantenna. *Nano Lett.* **2020**, *20*, 1992–1999.

(46) Gutiérrez-Arzaluz, L.; Ahmed, G. H.; Yang, H.; Shikin, S.; Bakr, O. M.; Malko, A. V.; Mohammed, O. F. Correlation of Photoluminescence and Structural Morphologies at the Individual Nanoparticle Level. *J. Phys. Chem. A* **2020**, *124*, 4855–4860.

(47) Froch, J. E.; Kim, S.; Mendelson, N.; Kianinia, M.; Toth, M.; Aharonovich, I. Coupling Hexagonal Boron Nitride Quantum Emitters to Photonic Crystal Cavities. *ACS Nano* **2020**, *14*, 7085–7091.

(48) Kim, S.; Fröch, J. E.; Christian, J.; Straw, M.; Bishop, J.; Totonjian, D.; Watanabe, K.; Taniguchi, T.; Toth, M.; Aharonovich, I. Photonic Crystal Cavities from Hexagonal Boron Nitride. *Nat. Commun.* **2018**, *9*, 2623.

(49) Schell, A. W.; Takashima, H.; Tran, T. T.; Aharonovich, I.; Takeuchi, S. Coupling Quantum Emitters in 2D Materials with Tapered Fibers. *ACS Photonics* **2017**, *4*, 761–767.

(50) Elshaari, A. W.; Skalli, A.; Gyger, S.; Nurizzo, M.; Schweickert, L.; Esmaeil Zadeh, I.; Svedendahl, M.; Steinhauer, S.; Zwiller, V. Deterministic Integration of HBN Emitter in Silicon Nitride Photonic Waveguide. *Adv. Quantum Technol.* **2021**, *4*, 2100032.

(51) Tran, T. T.; Wang, D.; Xu, Z. Q.; Yang, A.; Toth, M.; Odom, T. W.; Aharonovich, I. Deterministic Coupling of Quantum Emitters in 2D Materials to Plasmonic Nanocavity Arrays. *Nano Lett.* **2017**, *17*, 2634–2639.

(52) Bogdanov, S. I.; Shalaginov, M. Y.; Lagutchev, A. S.; Chiang, C.; Shah, D.; Baburin, A. S.; Ryzhikov, I. A.; Rodionov, I. A.; Kildishev, A. V.; Boltasseva, A.; Shalaev, V. M. Ultrabright Room-Temperature Sub-Nanosecond Emission from Single Nitrogen-Vacancy Centers Coupled to Nanopatch Antennas. *Nano Lett.* **2018**, *18*, 4837–4844.

(53) Bogdanov, S. I.; Makarova, O. A.; Xu, X.; Martin, Z. O.; Lagutchev, A. S.; Olinde, M.; Shah, D.; Chowdhury, S. N.; Gabidullin, A. R.; Ryzhikov, I. A.; Rodionov, I. A.; Kildishev, A. V.; Bozhevolnyi, S. I.; Boltasseva, A.; Shalaev, V. M.; Khurgin, J. B. Ultrafast Quantum Photonics Enabled by Coupling Plasmonic Nanocavities to Strongly Radiative Antennas. *Optica* **2020**, *7*, 463–469.

(54) Mendelson, N.; Xu, Z. Q.; Tran, T. T.; Kianinia, M.; Scott, J.; Bradac, C.; Aharonovich, I.; Toth, M. Engineering and Tuning of Quantum Emitters in Few-Layer Hexagonal Boron Nitride. *ACS Nano* **2019**, *13*, 3132–3140.

(55) Mendelson, N.; Doherty, M.; Toth, M.; Aharonovich, I.; Tran, T. T. Strain-Induced Modification of the Optical Characteristics of Quantum Emitters in Hexagonal Boron Nitride. *Adv. Mater.* **2020**, *32*, 1908316.

(56) Schell, A. W.; Tran, T. T.; Takashima, H.; Takeuchi, S.; Aharonovich, I. Non-Linear Excitation of Quantum Emitters in Hexagonal Boron Nitride Multiplayers. *APL Photonics* **2016**, *1*, 091302.

(57) Chen, B.; He, Z.; Liu, Z. J.; Wang, Y. K.; Gao, Y. N.; Aharonovich, I.; Xu, Z. Q.; Liu, J. Simultaneously Enhanced Linear and Nonlinear Photon Generations from WS₂ by Using Dielectric Circular Bragg Resonators. *Nanophotonics* **2020**, *9*, 2587–2592.